Journal of Rare Earths 36 (2018) 1310–1318

Contents lists available at ScienceDirect

Journal of Rare Earths

journal homepage: http://www.journals.elsevier.com/journal-of-rare-earths

Dielectric and microstructural properties of YAG:Dy^{3+} ceramics

Munirah Abdullah Almessiere [a, b, *], Bayram Unal [c], Abdulhadi Baykal [b]

[a] Department of Physics, College of Science, Imam Abdulrahman Bin Faisal University, P.O. Box 1982, 31441 Dammam, Saudi Arabia
[b] Department of Nanomedicine Research, Institute for Research & Medical Consultations (IRMC), Imam Abdulrahman Bin Faisal University, P.O. Box 1982, 31441 Dammam, Saudi Arabia
[c] Department of Software and Computer Engineering, Istanbul Sabahattin Zaim University, Halkali Cad. No: 2, Halkali, Kucukcekmece, 34303 Istanbul, Turkey

ARTICLE INFO

Article history:
Received 9 January 2018
Received in revised form
11 April 2018
Accepted 18 April 2018
Available online 10 August 2018

Keywords:
Yttrium aluminium garnet (YAG)
X-ray diffraction (XRD)
Conductivity
Dielectric properties
Rare earths

ABSTRACT

Yttrium aluminium garnet ($Y_3Al_5O_{12}$:YAG) singly doped with Dy^{3+} at different concentrations was prepared by solid state reactions using repeated heating cycles over the temperature range of 1300–1600 °C. X-ray powder diffraction analysis confirms the presence of a well-crystallized YAG perovskite phase with cubic structure (by Rietveld refinement). The rare earth dopant is successfully integrated into the YAG host lattice without any major changes in the original structure. The temperature dependence, up to 250 °C, of the conductivity, dielectric constant, dielectric loss, and loss tangent, at various frequencies of up to 5.0 MHz for undoped and doped crystals is compared to understand the electrical and structural characteristics. The experimental results reveal that Dy^{3+} dopants in YAG crystal significantly influence the conductivity, dielectric constant, and lossy mechanisms, which is probably due to the 3d-Al ions and 4f-Dy ions incorporated at different positions of both tetrahedral and octahedral symmetries in YAG:xDy^{3+} ceramics.

1. Introduction

Substitution in perovskite materials by rare earth and transition metal ions such as Gd, La, Nd, Pr, Sm and Co, Ni, Mn as active ions have been widely utilized in applications for improving optical, mechanical, magnetic, dielectric and ferroelectricity properties.[1,2] These properties mainly depend on the quantity of substitution, composition, fabrication methods, and temperature and time of sintering.[3] Yttrium aluminium garnet ($Y_3Al_5O_{12}$; YAG) ceramics are promising materials for resonators, antennae, and filters used for high frequency applications. For improving a higher frequency telecommunicating device, microwave/millimetre wave dielectric materials with both lower dielectric constant and greater quality factor (Qf) are required.[4,5] The fine dielectric properties of the single crystal indicate that dense YAG ceramics are also characterized by a high Qf value.[6] In addition, above all, the comprehensive study in both optical and dielectric properties of Dy-doped YAG presents a crucial importance over a wide range of thermographic application enabling surface temperatures measurable over a wide range extending from sub 0 °C up to over 1400 °C by exploiting the temperature-dependent luminescence of any lanthanide-doped YAG.[7] In general, YAG is synthesized through a solid-state reaction above 1600 °C.[7]

YAG doped with a transition metal or lanthanide element is an important class of solid-state laser material widely used in luminescence systems and as window material for a variety of lamps.[8] The electrical conductivity of YAG is also reported to be lower than that of any other polycrystalline oxide.[9] YAG ceramics doped with rare earths are extensively used to achieve high dielectric performance and low dissipation factor of the capacitors.[10] The incorporation of trivalent rare-earth cations such as La^{3+}, Dy^{3+}, Sm^{3+}, Er^{3+}, and Ho^{3+} in the perovskite lattice modifies the microstructure and electrical properties of doped YAG.[11] The larger ionic size rare-earth ions (La, Sm) predominantly dissolve in A-sites and act as donors, and the intermediate ionic size rare-earth ions (Dy, Ho, Er) dissolve in both A- and B-cationic lattice sites depending on their concentration and may act as donors or/and acceptors.[12] The dysprosium ion (Dy^{3+}), shows amphoteric behaviour and can occupy both A and B cationic sites in the crystal structure. Dy^{3+} ions incorporated at A sites act as donors whereas those incorporated at B sites act as acceptors. The degree of Dy^{3+} ion incorporation at A and/or B sites depends on the A/B ratio.[13,14] In this study, YAG:Dy ceramics via solid state reaction method was

* Corresponding author. Department of Physics, College of Science, Imam Abdulrahman Bin Faisal University, P.O. Box 1982, 31441 Dammam, Saudi Arabia.
E-mail address: malmessiere@iau.edu.sa (M.A. Almessiere).

https://doi.org/10.1016/j.jre.2018.04.011
1002-0721/

synthesized and their microstructure and dielectric properties were investigated.

2. Materials and methods

The Dy-doped YAG samples were prepared by a solid state route. Y_2O_3 (99.9%, US-Nano) and Al_2O_3 (99.9%, US-Nano) powders were used as starting materials for preparation of $Y_3Al_5O_{12}$ (YAG) at a chemical ratio of 3:5. For preparation of Dy^{3+} doped YAG (YAG:*x*Dy; x = 0.01 wt%, 0.05 wt%, 0.07 wt%, and 0.09 wt%) samples, the stoichiometric amount of Dy_2O_3 (99.9%, US-Nano) was added to YAG, mixed well, ground within an agate mortar, and then compressed into pellets. After that each pellet was placed in an Al crucible and then sintered at 1300, 1500 and 1600 °C for 5 h subsequently. Between each heating step, pellet was ground, made pellet and sintered. Finally, the products were cooled to room temperature.

The structure of the phosphor samples was studied by X-ray powder diffraction using a Shimadzu XRD 6100 X-ray diffractometer (Cu Kα radiation, $\lambda = 0.1540$ nm). For electrical measurement, silver paste was applied as electrodes on both sides of the pellets. The electrical properties were studied by impedance spectroscopy (IS) measurements performed on the sintered materials using Novocontrol concept 50 system in the $1–10^6$ Hz frequency range. The IS measurements were performed at different temperatures where the temperature was controlled by the Quatro cryosystem. The samples were imaged in Teneo VS SEM (Thermo Fisher Scientific) at an accelerating voltage of 1.0 kV, probe current of 100 pA and working distance of 5 mm in Optiplan mode. The magnification range was from 1000× to 100 000× with 3 different detectors.

3. Results and discussion

3.1. XRD analysis

Fig. 1(a,b) presents the XRD pattern of pure $Y_3Al_5O_{12}$ phosphor measured according to the database in Match!3 with card number [96-152-9038]. A well-crystallized YAG phase is deduced. There is minor amount of secondary phase of $YAlO_3$ (YAP) in the product. First, it formed an Al_2O_3 rich $Y_4Al_2O_9$ (YAM) phase in low temperature range (900–1100 °C). Then, it transformed into a YAP phase upon increasing the temperature from 1100 to 1250 °C. Finally, it was converted to YAG by reacting with Al_2O_3 ions at elevated temperature (1250–1700 °C). Cubic structure of the obtained YAG has been confirmed by Rietveld refinement using Match!3 and Diamond software.

Based on our experimental measurements as seen in Fig. 1(a), all the typical diffraction peaks match with cubic crystal structure of YAG phase. Y and Al atoms have the same atomic coordinate while oxygen atoms have different atomic coordinates. This indicates that the orientation of the crystal structure has changed. Similarly, the effects of doping Dy^{3+} ions into YAG phosphor are shown in Fig. 1. As shown, no impurity phase is detected, which implies that Dy^{3+} ions merged into the host lattice even when the content of Dy^{3+} ions was increased. XRD patterns of the doped samples reveal a slight shift toward smaller angles compared to the pure sample. However, as Dy^{3+} substitution increases, the intensity of XRD peaks decreases for $x = 0.05$, 0.07 and 0.09 due to the low crystallinity of the product (Fig. 1(b)). Upon increasing the Dy^{3+} concentration, the lattice parameters that were recorded show a slight increase (1.20044, 1.20050, 1.20053, 1.20052 1.20056 nm for $x = 0.00$, 0.01, 0.05, 0.07, and 0.09, respectively). The changes in the cell parameters are due to the difference in the average ionic radii of Dy^{3+} (0.103 nm) and Y^{3+} (0.101 nm) ions. Hence, the ionic size of the Dy^{3+} ion is higher than that of the Y^{3+} ion. This causes a shift in the XRD pattern, as reported previously.[6] In fact, the concentration of the doped ions has an influence on the lattice parameters of the crystal owing to the difference in the ionic size of the ions.

3.2. Morphology investigation

SEM micrographs of $Y_3Al_5O_{12}$ ($Y_{3-x}Dy_xAl_5O_{12}$ ($0.00 \le x \le 0.09$)) have been performed in different areas of the samples at various magnifications. Intermediary magnification was chosen as shown in Fig. 2. The images display regular aggregates of spheres structure.

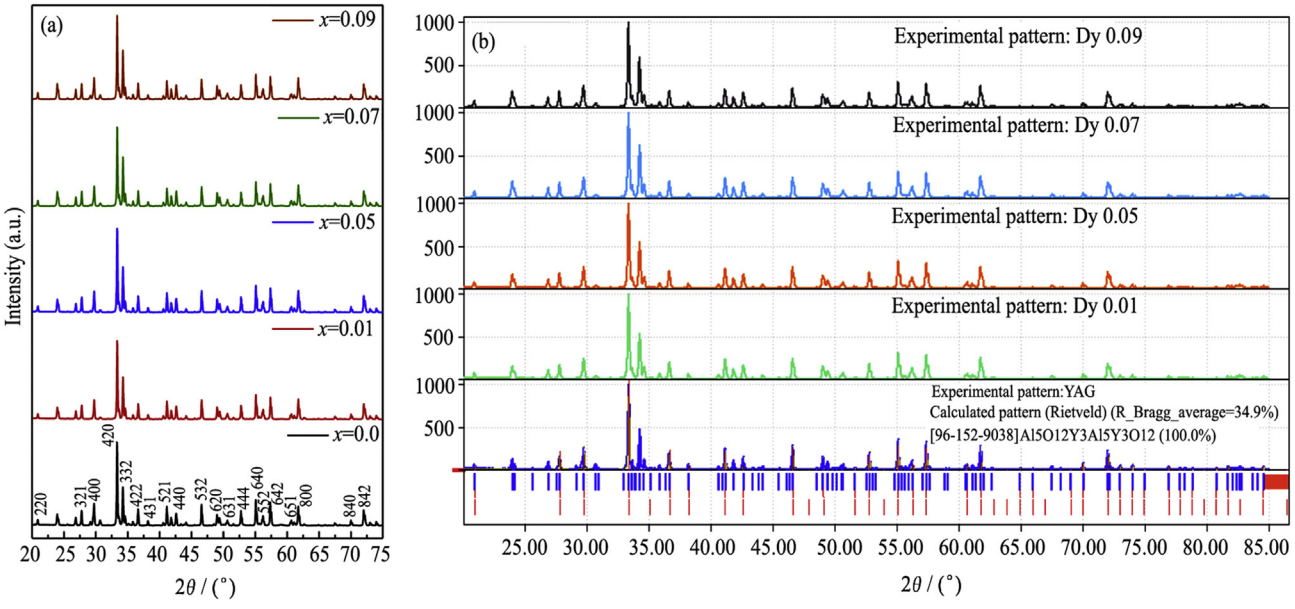

Fig. 1. XRD patterns (a) and Rietveld refinement (b) of $Y_{3-x}Dy_xAl_5O_{12}$ ($0.00 \le x \le 0.09$).

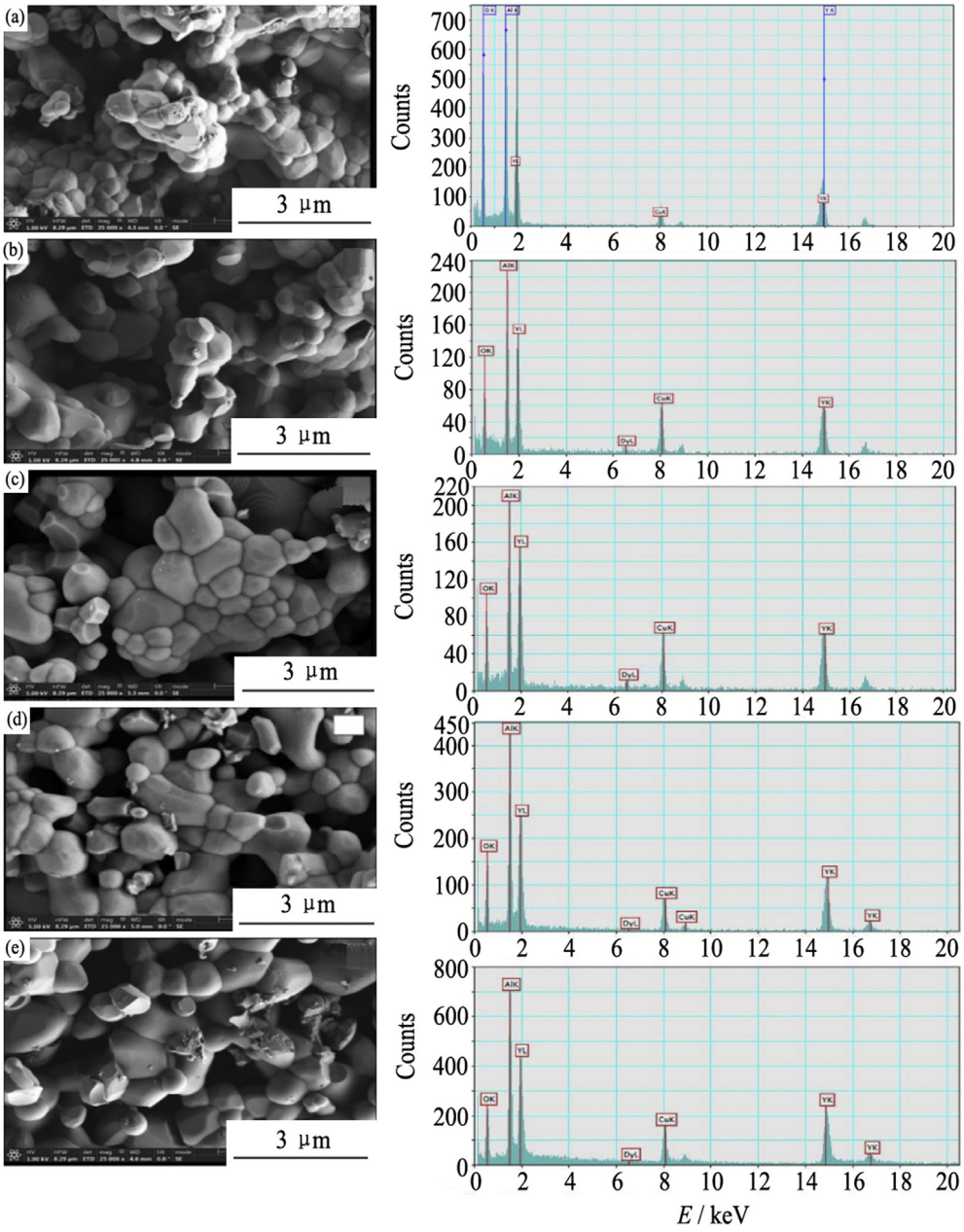

Fig. 2. SEM images along with EDX spectra of $Y_{3-x}Dy_xAl_5O_{12}$ ($0.00 \leq x \leq 0.09$). (a) $x = 0$; (b) $x = 0.01$; (c) $x = 0.05$; (d) $x = 0.07$; (e) $x = 0.09$.

We observed a variation in spherical size from $x = 0.0$ to $x = 0.09$, which exhibits an increase in diameter. The EDX spectra revealed the presence of Y, Al, Dy, and O in all samples (except $x = 0.0$). The average grain size of all products is between 500 nm and 2 μm.

3.3. Electrical conductivity and dielectric behaviour

YAG is a garnet-structured oxide, therefore, both yttrium and two aluminium cations are located at positions of different symmetries. Here yttrium ions occupy the centre of a dodecahedron surrounded by eight oxygen atoms. Al ions reside in two positions of different symmetries within the YAG lattice. Al atoms in yttrium aluminium garnet occupy two positions, one with a group symmetry of one octahedral point and another with a group symmetry of tetrahedral point. Therefore, a complementary compound of the lattice cell is built up quite largely, and so the cell comprises 8 structural formulae or 160 atoms. This complex structure of the YAG can be considered as a network of interconnected octahedra, tetrahedra, and dodecahedra, in which aluminium atoms are surrounded by oxygen atoms at the corners, so that each oxygen atom is a member of two dodecahedra, one octahedron, and one tetrahedron.[14] Further, the dielectric characteristics of a YAG crystal are isotropic because of its cubic symmetry. Any electrical characteristics and dielectric behaviour of some compound materials, such as lanthanide-doped YAG, could be interpreted by any percolation approach taken in several domains for various electrical methodology. The well-known Fourier transformation can also deconvolute the response to a sinusoidal stimulus to evaluate the complex impedance. Therefore, it can be noted that complex dielectric constant is presented by Eq. (1) [15,16]:

$$\varepsilon^*(\omega;T) = \varepsilon'(\omega;T) - i\varepsilon''(\omega;T) \quad (1)$$

Further, the complex conductivity is calculated with the following equation:

$$i\sigma^*(\omega;T) = \sigma'(\omega;T) - i\sigma''(\omega;T) \quad (2)$$

where, ω is the angular frequency of the bias potential difference across the coupled electrodes. The ac conductivity (σ_{ac}), dielectric constant (ε'), dielectric loss (ε''), and tangent (tanδ) loss can be examined using the standard relation,

$$\varepsilon\prime = \frac{Cd}{\varepsilon_0 A} \quad (3)$$

where, C is the electrode capacitance in Farad (F), A a cross-sectional area of the pellet in m^2, d the gap between the two coupled electrodes, and ε_0 (=8.852 × 10^{-14} F/cm) the dielectric permittivity of vacuum. It can be realized that the real part of ac conductivity is acquired from the imaginary part of the dielectric loss $\varepsilon''(\omega)$ relative to the expression, $\varepsilon'' = \varepsilon'\tan\delta$ and is also expressed as,

$$\sigma_{ac} = \omega\varepsilon_0\varepsilon'' = \omega\varepsilon_0\varepsilon' \tan\delta \quad (4)$$

where, ε'' is also termed the imaginary part of complex dielectric permittivity (ε^*). In addition, it is realized that the evaluated frequency dependence of conductivity is useful to determine the electrical transportation in a variety of compound materials. In general, the conductivity is assigned to two components in most compositions of YAG:xDy. The first component is dc conductivity owing to "band conduction" and the second component is ac conductivity due to "hopping mechanism" between the ions of the same element, for instance Al, occurring in more than one valence states. Here, a power law dependency is represented with a certain power exponent as illustrated in the power law equation in the following section. All aforementioned theoretical evaluations, that is, ac/dc conductivities (σ_{ac}/σ_{dc}), dielectric constant (ε') and dielectric loss (ε''), dielectric tangent loss, and finally dielectric modulus were examined as functions of frequency, compositional ratios of x = 0.00, 0.05, 0.07, 0.09 and temperature up to 250 °C using an impedance analyser in the frequency range up to 5.0 MHz.

3.4. Conductivity

The measurement of ac conductivity (σ_{ac}) of the YAG:xDy^{3+} ceramics (x = 0.0, 0.05) as a function of frequency was performed in the temperature range of 20–250 °C as mentioned earlier. The frequency dependence of conductivity for YAG:xDy^{3+} ceramics in Fig. 3(a,b) was calculated from the standard equation expressed as,[15]

$$\sigma'(\omega;T) = \sigma_{ac}(\omega;T) = \varepsilon''(\omega;T)\omega\varepsilon_0 \quad (5)$$

where, $\sigma'(\omega;T)$ is the real component of complex conductivity, ε'' the imaginary part of complex dielectric permittivity (ε^*), ε_0 the vacuum permittivity, and ω the angular frequency of ac stimulation signal applied across the sample as mentioned earlier. The ac conductivities of a variety of YAG:xDy^{3+} ceramics ($0.00 \le x \le 0.09$) as a function of frequency, up to 1 MHz, for various temperatures ranging up to 250 °C is shown in Fig. 3(c). Clearly, pure YAG and all the doped YAG ceramics show a linear tendency in the log–log graphs, regardless of the dopant (Dy) concentration, which implies that the conductivity tends to vary with the power exponent law of frequencies, as follows:

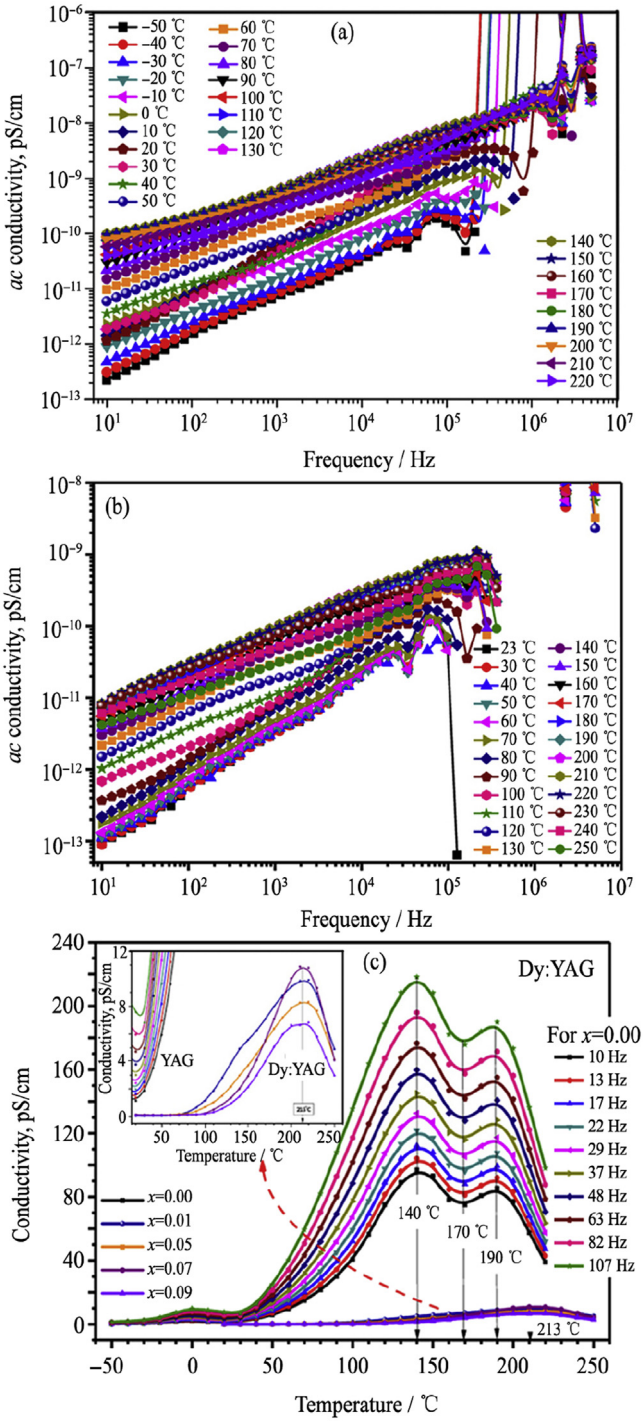

Fig. 3. (a, b) ac Conductivity versus frequency of YAG:xDy^{3+} (x = 0.0, 0.05). (c) dc Conductivity versus temperature for different Dy^{3+} concentration.

$$\sigma(w,T,x) = \sigma_0(T,x)\omega^n \quad (6)$$

where, $\sigma_0(T,x)$ denotes both temperature and dopant-dependent proportionality pre-coefficient of ac conductivity and $n(T,x)$ is the power exponent which can vary with both temperature and doping concentration level with reference to the curve of pure YAG. The power exponent is therefore calculated easily from the slope of the graphs of lgσ_{ac} versus lgω for each of the four substitutions. When

the tendencies of all the curves are examined carefully, fluctuations occur at higher frequencies. However, the fluctuation level shifts up and down as the dopant concentration, frequency, and temperature are increased. Better variation of the regular tendencies is especially presented for pure YAG and YAG:xDy^{3+} with $x = 0.07$, almost reaching up to 10 kHz while others start to fluctuate earlier. Because of the detailed analysis of the last graph, it should be emphasized that both dc conductivity is considered at the lowest frequency of 10 Hz for a variety dysprosium substitution including the pure one for comparison. The ac conductivity of pure YAG at some lower frequencies up to 107 Hz provides many insights on the influence of dysprosium ion doping on the conductivity of YAG. It is clearly noted that the dc conductivity at the lower frequency of 10 Hz increases sharply up to a value of 210 pS/cm, reaches a maximum value with various tendencies at temperatures up to 140 °C as shown in Fig. 3(c). Then, it slightly decreases corresponding to a temperature of 170 °C. Subsequently, the curve reaches another peak value at 190 °C, while the conductivity of the doped ceramics shifts to a higher temperature with a single maximum value at ~213 °C, regardless of the level of dysprosium substitution. However, the dc conductivity of pure YAG ceramics realizes twin values of the peak of 97 pS/cm centred at 140 °C and of 86 pS/cm centred at 190 °C, while that of all YAG:xDy ceramics achieves only single peak between 7 and 11 pS/cm at 213 °C, again, as depicted in Fig. 3(c). Therefore, we can summarize that dc conductivity depends on any doping levels with a complicated up-and-down tendency. This type of variation might be due to some contribution of "small polaron hopping" to the conductivity. This obviously implies that the conduction phenomenon is ac conduction due to the hopping of charge carriers across the sites. In general, the conductivity of non-doped YAG decreases quickly with any level of the substitutional dysprosium ions while it is strongly dependent on both temperature and frequencies. These types of tendencies could be considered for a general dielectric behaviour and can be explained on the basis that the hopping conduction increases at higher frequencies while some charges from different trapping centres are released, which supports hopping electron conduction between octahedral and tetrahedral symmetries of aluminium to be the conduction mechanism, as mentioned earlier. Beyond these discussions, there is not much information based on dielectric properties of YAG:xDy^{3+} ceramics in the literature, except for optical properties[16–18] (Fig. S1(a–e) show ac conductivity characteristics of YAG:xDy^{3+} ($0.00 \leq x \leq 0.09$) as a function of frequency for various temperatures up to 250 °C, (f) shows both dc conductivity at the lowest frequency at 10 Hz for different Dy^{3+} concentrations including the pure one for comparison and the lower frequency conductivity of pure YAG at frequencies between 10 and 107 Hz, as depicted in the legend).

3.5. Dielectric constant

Generally, the dielectric constant decreases with increasing frequencies up to a value of 5.0 MHz, whereas increasing with the increase of temperature, which is especially more evident for undoped YAG. So, the variation of dielectric constant is regulated easily with the substitutional Dy ions. The characteristics of the dielectric constant of $Y_{3-x}Dy_xAl_5O_{12}$ (x = 0.0, 0.09) are shown in Fig. 4 as a function of frequency for various temperatures up to 250 °C. As shown, the dielectric constant reduces with a multi-exponential tendency rather than either a power exponent or simply-exponential tendency. The substitutional dysprosium causes a slight reduction in dielectric constant while the influence of temperature over dielectric constant results in a larger variation at lower frequency. However, the dielectric constant remains almost unchanged at higher frequency. Additionally, the frequency of

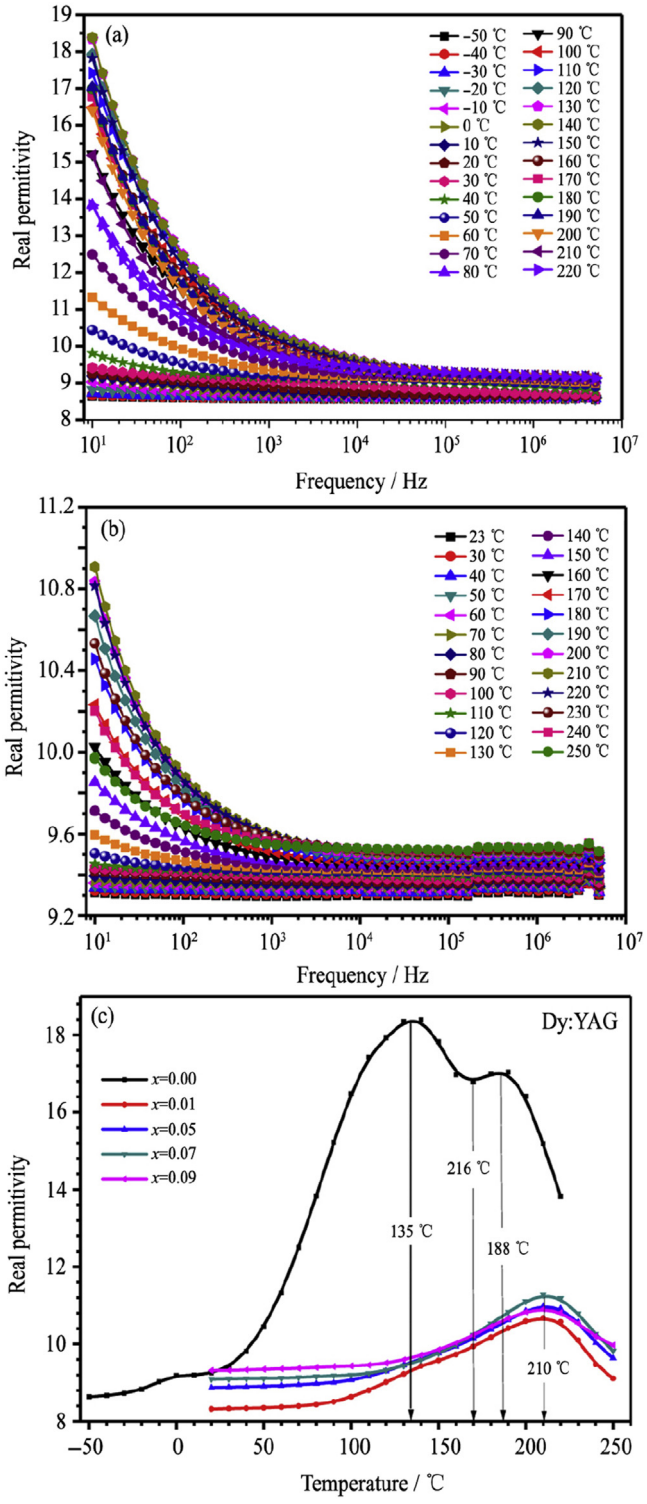

Fig. 4. (a, b) The dielectric constant versus frequency of $Y_{3-x}Dy_xAl_5O_{12}$ (x = 0.0, 0.09); (c) The dielectric constants versus temperature with various Dy^{3+} concentrations.

applied ac signal has a significant effect on dielectric constant of both pure and doped ceramics. In general, pure and doped ceramics leads to no significant tendencies with respect to the real part. When the dependence of dielectric constant on the lowest frequency is examined in detail from the perspective of temperature dependency, the characteristics of the doped ceramics is found to be completely different from those of the pure one. Additionally, YAG shows a doublet peak located at 135 and 188 °C while all the

doped ones show a single shifted peak centred at ~210 °C regardless of the dopant level, as depicted in Fig. 4(c). For all substitutions up to 0.09, the dielectric constant as a function of temperature for the entire frequency region shows some different characteristics. This is attributed to the electrical conduction due to both electron and polaron hopping mechanisms. Because of the complexity of a variety of studied YAG:xDy^{3+} ceramics, as mentioned earlier for two types of symmetries, the dielectric constant depends on how fast the level of polarization organizes itself to communicate with the stimulus of an externally applied electric field oscillations. As the frequency is increased, the polarization orientation is reduced, because the alignment of dipole moments requires a longer interval of the response time compared with the orientation of the electronic and ionic polarizations. This gives rise to a reduction in the dielectric constant, and the reduction rate varies for all the samples depending on the frequency, temperature, and substitutional ratio of the lanthanide ions. The frequency dependence of the dielectric constant discloses the presence of electrode interface polarization processes, which usually appear at lower frequencies. The incremental temperature dependency, in general, could be attributed to the molecular orientation and arrangement.[19] Thus, the dielectric constant of YAG:xDy^{3+} ($0.00 \leq x \leq 0.09$) increases with temperature because of the improvement in the boundaries among the lanthanide ion substitutions in YAG due to changing dopant concentration (Fig. S2(a–e) show the characteristics of the dielectric constant of YAG:xDy^{3+} ($0.00 \leq x \leq 0.09$) as a function of frequency for various temperatures up to 250 °C, (f) shows the dielectric constants at the lowest frequency of 10 Hz for phosphors with various Dy^{3+} concentrations including the pure one for comparison, as mentioned in the legend).

3.6. Dielectric loss

In general, the dielectric loss for both undoped and Dy^{3+}-doped YAG ceramics displays a power law tendency i.e., almost a linear curve in the log-log plots. The temperature and frequency dependency curves show a highly linear decrease with respect to the frequency up to 5 MHz, which is more noteworthy at higher temperatures. On the contrary, this curve shows a variety of tendencies at higher frequencies depending on the concentration of the Dy^{3+} ions. This linearity overall the frequency range of the log-log plots is related to the power law with an exponent, as defined by,

$$\varepsilon''(\omega;T) = \varepsilon''(0;T)\omega^{n} \tag{7}$$

where, ω is the angular frequency and $\varepsilon''(0;T)$ is the pre-coefficient dielectric loss that is strongly dependent on the temperature, as shown in Fig. 5(a–c). n is the power exponent correlated with the temperature and substitution of lanthanide Dy^{3+} ions in YAG and YAG itself, as illustrated in Fig. 5(a). It is also evident that the capacitive response exhibits a higher temperature dependence compared to the nature of reorganization of Dy^{3+} ions doped in YAG. This linearity in the log–log plots corresponds to dc conductance (σ_{dc}), expressed as,

$$\varepsilon''_{dc} = \sigma_{dc}(\omega C_o) \tag{8}$$

where, C_o is the vacuum capacitance. The dielectric loss ultimately reaches a minimum at a higher frequency with some fluctuations, and shifts to higher side of frequency in general, being dependent upon the substitutional ratio of the lanthanide ions in YAG. Owing to charge transfer between the octahedral and tetrahedral symmetries of aluminium ions, a limited drift motion of charges occurs in the direction of the externally applied electric field, which establishes the polarization. The degree of polarization reduces with

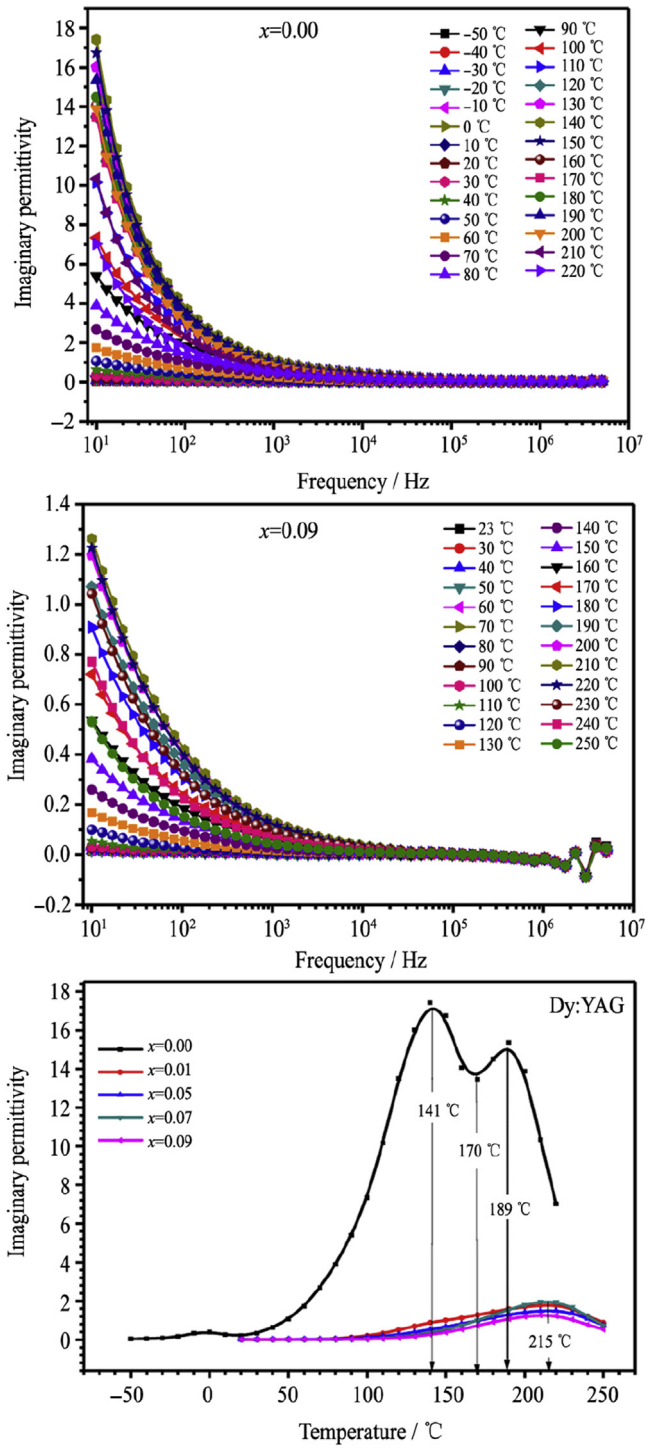

Fig. 5. (a, b) The dielectric loss versus frequency of $Y_{3-x}Dy_xAl_5O_{12}$ (x = 0.0, 0.09); (c) The dielectric loss versus temperature for various Dy^{3+} concentrations.

increasing frequency because the electronic transition between the octahedral and tetrahedral symmetries of aluminium ions delays the following electric field. The dielectric loss of $Y_{3-x}Dy_xAl_5O_{12}$ (x = 0.0, 0.09) as a function of frequency for various temperatures up to 250 °C is illustrated in Fig. 5(a,b). As observed, the dielectric loss decreases with a multi-exponential tendency as in the case of the real part, rather than showing a simple exponential tendency. Yet, the dysprosium dopant induces a slight reduction in the dielectric constant while the temperature effect leads to a bigger

variation at lower frequencies; however, the dielectric constant remains almost unchanged at higher frequencies. Further, the frequency of the applied ac signal significantly influences the dielectric constant for both pure and doped samples. In general, the imaginary part of pure (~10) and dopant samples (~1.8), regardless of the dopant level, shows substantial changes when compared with the corresponding real part. For the dopant concentration of $x = 0.07$, it shows a slight difference from others showing a higher value. When electrical tendency for temperature dependency is examined dielectrically under a lower frequency range within a lossy perspective, the characteristics of the doped samples is altered completely from those of the YAG. Additionally, YAG sample contains a doublet peak located at 141 and 189 °C while all the doped ones, regardless of their level, have a single shifted peak centred at about 215 °C, as depicted in Fig. 5(c) (Fig. S3(a–e) show the characteristics of the dielectric loss of YAG:xDy^{3+} ($0.00 \leq x \leq 0.09$) as a function of frequency for various temperatures up to 250 °C, (f) shows dielectric loss at the lowest frequency of 10 Hz for phosphors with various Dy^{3+} concentrations including the pure one for comparison, as mentioned in the legend).

3.7. Dielectric modulus

The dielectric modulus can be divided into both real and imaginary components of complex dielectric data relevant to the dielectric constant ε' and dielectric loss ε'' and then expressed in the form of,[20,21]

$$M^* = \frac{1}{\varepsilon^*} = M' + iM'' = \frac{\varepsilon' + i\varepsilon''}{\varepsilon'^2 + \varepsilon''^2} \quad (9)$$

where, M' and M'' are the real and complex components of the dielectric modulus, respectively.

The real Modulus of both undoped and Dy^{3+} ion-doped YAG ceramic versus frequencies of up to 5.0 MHz for temperatures ranging from 23 to 250 °C is summarized in the form of graphs in Fig. 6(a,b). It is important to emphasize that the real modulus increases with incremental frequency, obeying a type of power law. It is also noteworthy that less variation is observed at higher frequencies for all temperatures. At lower temperatures, the real modulus shows a considerably high variation in magnitude while a small variation is only observed at higher frequency, especially after medium frequencies, say being greater than 1 kHz. However, it is almost independent of temperature for higher frequency, which implies that all the curves are saturated, wherein the saturation and dependency are also relevant to the level of substitutions. It is important to note that the temperature dependency is considerably high at lower frequencies for all samples but especially for undoped YAG. Fig. 6(c) also shows the significant variation between the undoped and doped samples at a frequency of 10 Hz. The curve of real modulus for pure YAG ceramics exhibits double minima at temperatures of both 140 and 190 °C whereas a single minimum is observed at about 213 °C for all the doped YAG. We can conclude that a small amount of Dy^{3+} ions doped in YAG structure produces an important effect on modulus attitudes (Fig. S4(a–e) show the characteristics of real modulus of YAG:xDy^{3+} ($0.00 \leq x \leq 0.09$) as a function of frequency for various temperatures up to 250 °C, (f) depicts both the real modulus at the lowest frequency of 10 Hz for phosphors with various Dy^{3+} concentrations including the pure one for comparison and that of pure YAG at the frequency of 10 Hz shown in the legend).

The imaginary modulus of both undoped and Dy^{3+}-doped YAG versus frequencies of up to 5.0 MHz for temperatures ranging from 23 to 250 °C is shown in Fig. 7(a,b). For undoped YAG, the imaginary modulus decreases rapidly with the frequency up to

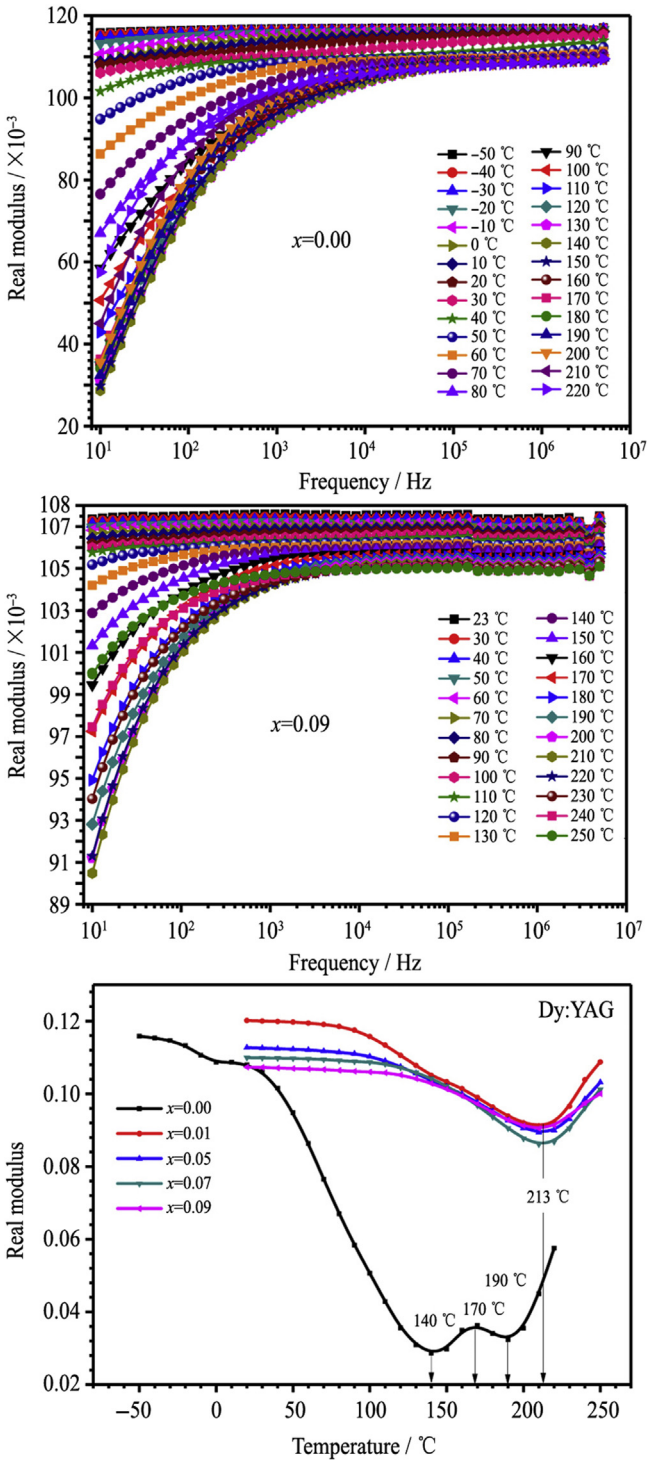

Fig. 6. (a, b) The real modulus versus frequency for $Y_{3-x}Dy_xAl_5O_{12}$ ($x = 0.0, 0.09$); (c) The real modulus versus temperature for various Dy^{3+} concentrations.

100 kHz and then it fluctuates at the highest frequency over 2.0 MHz. For the Dy^{3+}-doped YAG ceramics, it reduces rapidly with the frequency up to 1 kHz when the doping level is increased up to $x = 0.09$. Further, the temperature dependency at the low frequency of 10 Hz is quite large for the YAG ceramic compared to doped samples. When the graphs of Fig. 7(c) are examined, the undoped sample presents three valleys centred at the temperatures of 130, 171, and 216 °C (drop) whereas the modulus

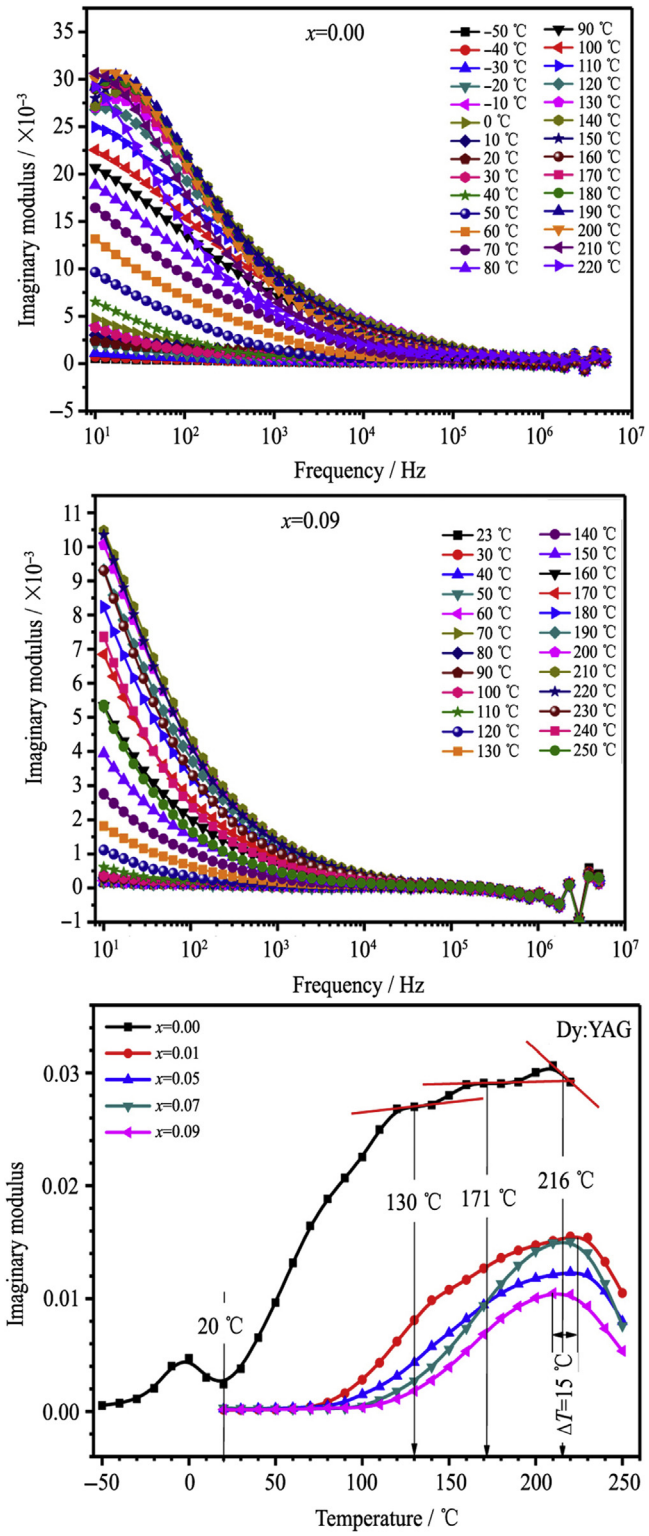

Fig. 7. (a, b) The imaginary modulus versus frequency for $Y_{3-x}Dy_xAl_5O_{12}$ (x = 0.0, 0.09); (c) The imaginary modulus versus temperature for various Dy^{3+} concentrations.

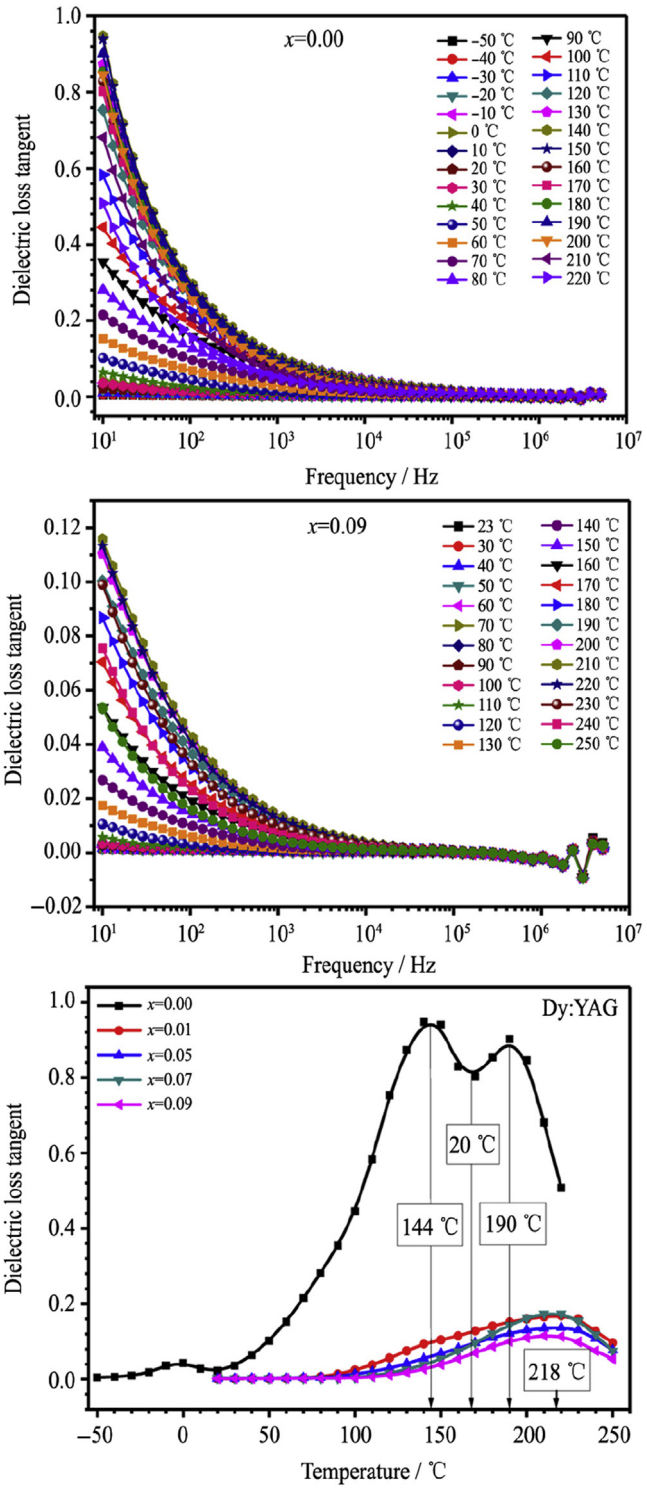

Fig. 8. (a, b) The dielectric loss tangent characteristics versus frequency for $Y_{3-x}Dy_xAl_5O_{12}$ (x = 0.0, 0.09); (c) The imaginary dielectric constant versus temperature for various Dy^{3+} concentrations.

increases with temperature and reaches a maximum. Additionally, doped samples show less dependency on the temperature depending on the doping level. Clearly, it increases to a same maximum value of ~216 °C with a band shift of 15 °C in relation to the dopant dependencies (Fig. S5(a–e) show the characteristics of the imaginary modulus of YAG:xDy^{3+} ($0.00 \leq x \leq 0.09$) as a function of frequency for various temperatures up to 250 °C, (f) shows both imaginary modulus taken at lowest frequency at 10 Hz for a variety of given dysprosium concentration including pure one for comparison and that of pure YAG at frequency of 10 Hz shown in the legend).

3.8. Dielectric tangent loss

The characteristic evaluation of the dielectric loss tangent of $Y_{3-x}Dy_xAl_5O_{12}$ ($x = 0.0, 0.09$) is depicted in Fig. 8(a,b) as a function of frequency for various temperatures up to 250 °C. The dielectric loss tangent clearly decreases with a multi-exponential tendency rather than a simple exponential one. Yet, the dysprosium dopant introduces a significant reduction in loss while the temperature effects lead to a bigger variation at lower frequencies; however, dielectric loss tangent remains almost unchanged at higher frequencies. Moreover, the frequency of the applied ac signal significantly influences the loss for both pure and doped samples. In general, the dielectric loss tangent of doped samples (~0.13), regardless of the dopant level, is substantially modified compared with pure sample (~0.98). When the dielectric loss tangent is evaluated carefully under the lowest frequencies within the lossy perspective for temperature dependency, the characteristic of the doped samples is altered completely from those of the pure one. Additionally, YAG samples show a doublet peak centred at 144 and 190 °C whereas all the doped ones, regardless of their dopant level, show a single shifted peak located at ~218 °C, as depicted in Fig. 8(c) (Fig. S6(a–e) show dielectric loss tangent characteristics of YAG:xDy^{3+} ($0.00 \leq x \leq 0.09$) as a function of frequency for various temperatures up to 250 °C, (f) shows imaginary dielectric constant taken at lowest frequency of 10 Hz for a variety of Dy^{3+} ions concentration including pure one for comparison as depicted in the legend).

4. Conclusions

In this study, the dielectric and microstructural properties of YAG:xDy^{3+} ($0.00 \leq x \leq 0.09$) ceramics were investigated. The structural characterization indicates that the synthesized samples are uniform with good quality of crystallization. The electrical and dielectric properties of $Y_3Al_5O_{12}$ ceramics including those of the counterparts doped by various concentrations of Dy^{3+} ions were evaluated extensively from the perspective of the substitutional effect of the 4f-ions of the lanthanide-doped YAG ceramics. The temperature dependence of the conductivity, dielectric constant, dielectric loss, and loss tangent at various frequencies of up to 5.0 MHz for doped Dy^{3+} ions in YAG are responsible for various influences in the conductivity, dielectric constant, and loss mechanisms, which can be attributed to various lattice locations such as 3d-Al ions and 4f-Dy ions in both tetrahedral and octahedral symmetry in YAG:xDy^{3+} ceramics.

Appendix A. Supplementary data

Supplementary data related to this article can be found at https://doi.org/10.1016/j.jre.2018.04.011.

References

1. Sajjad A, Muhammad Azhar K, Mansoor S, Aziz ur R, Muhammad Farooq W, Imran S. The impact of Yb and Co on structural, magnetic, electrical and photocatalytic behavior of nanocrystalline multiferroic $BiFeO_3$ particles. *Ceram Int*. 2017;43(18):16880.
2. Lodhi MY, Khan MA, Akhtar MN, Warsi MF, Mahrmood A, Ramay SM. Role of Nd–Ni on structural, spectral and dielectric properties of strontium–barium based nano-sized X-type ferrites. *Ceram Int*. 2018;44(3):2968.
3. Huma M, Muhammad Azhar K, Altaf H, Muhammad Farooq W, Asif M, Shahid MR. Structural, spectral, thermal and dielectric properties of Nd–Ni co-doped Sr–Ba–Cu hexagonal ferrites synthesized via sol–gel auto-combustion route. *Ceram Int*. 2018;44(1):605.
4. Ohsato H. Research and development of microwave dielectric ceramics for wireless communications. *J Ceram Soc Jpn*. 2005;113(1323):703.
5. Krupka J, Derzakowski K, Tobar M, Hartnett J, Geyer RG. Complex permittivity of some ultralow loss dielectric crystals at cryogenic temperatures. *Meas Sci Technol*. 1999;10:387.
6. Kagomiya I, Matsuda Y, Kakimoto K, Ohsato H. Microwave dielectric properties of YAG ceramics. *Ferroelectrics*. 2009;387(1):1.
7. Chong JY, Zhang YL, Wagner B, Kang ZT. Co-precipitation synthesis of YAG:Dy nanophosphor and its thermometric properties. *J Alloys Compd*. 2013;581(12):484.
8. Ikesue A, Kamata K, Yoshida K. Fabrication and optical properties of high-performance polycrystalline Nd:YAG ceramics for solid-state lasers. *J Am Ceram Soc*. 1995;78(4):1033.
9. Kareiva AJ, Harlan CB, MacQueen DL, Cook RR, Barron A. Carboxylate-substituted alumoxanes as processable precursors to transition metal-aluminum and lanthanide-aluminum mixed-metal oxides: atomic scale mixing via a new transmetalation reaction. *Chem Mater*. 1996;8(9):2331.
10. Park JK, Kim HC, Yoon JY, Song MS, Kim TY, Hur HK. Doping behaviours of dysprosium, yttrium and holmium in $BaTiO_3$ ceramics. *J Eur Ceram Soc*. 2009;29(9):1735.
11. Qi JQ, Gui ZL, Wang YL, Zhu Q, Wu YJ, Li LT. The PTCR effect in $BaTiO_3$ ceramics modified by donor dopant. *Ceram Int*. 2002;28(2):141.
12. Paunović V, Živković Lj, Mitić V. Influence of rare-earth additives (La, Sm and Dy) on the microstructure and dielectric properties of doped $BaTiO_3$ ceramics. *Sci Sinter*. 2010;42:69.
13. Yamaji A, Enomoto Y, Kinoshita K, Murakami T. Preparation, characterization, and properties of Dy-doped small-grained $BaTiO_3$ ceramics. *J Am Ceram Soc*. 1977;60(3–4):97.
14. Lee WH, Groen WA, Schreinemacher H, Hennings D. Dysprosium doped dielectric materials for sintering in reducing atmospheres. *J Electroceram*. 2000;5(1):31.
15. Auwal A, Unal I, Güngüneş H, Shirsath ES, Baykal A. Dielectric properties, cationic distribution calculation and hyperfine interactions of La^{3+} and Bi^{3+} doped strontium hexaferrites. *Ceram Int*. 2016;42(7):9100.
16. Ahmed MA, Mansour SF, El-Dek SI, Karamany MM. Hybridization between microstructure and magnetization improvement in lead and RE co-doped $BiFeO_3$. *J Rare Earths*. 2016;34(5):495.
17. Trajic J, Rabasovic SM, Savic-Sevic S, Sevic D, Babic B, Romcevic M, et al. Far-infrared spectra of dysprosium doped yttrium aluminum garnet nanopowder. *Infrared Phys Technol*. 2016;77(7):226.
18. Cao XQ, Li XL, Chen XW, Xu SL, Xiong DK, Deng W. Preparation, characterization and optical properties of Dy-doped yttrium aluminum garnet. *Int J Mod Phys B*. 2017;31(16–19):1.
19. Klimczak M, Malinowski M, Sarnecki J, Piramidowicz R. Luminescence properties in the visible of Dy:YAG/YAG planar waveguides. *J Lumin*. 2009;129(12):1869.
20. Zorenko Y, Gorbenko V, Zorenko T, Banaszak A, Mosinska L, Paprocki K, et al. Luminescent and scintillation properties of YAG:Dy and YAG:Dy,Ce single crystalline films. *Radiat Meas*. 2016;90(7):308.
21. Sözeri H, Genç F, Unal B, Baykal A, Aktas B. Magnetic, electrical and microwave properties of Mn–Co substituted $Ni_xZn_{0.8-x}Fe_2O_4$ nanoparticles. *J Alloys Compd*. 2016;660(5):324.